PROCEEDINGS OF SCIENCE

Searches for Gamma Ray sources with GRAPES-3

M. Karthik[a,*],M. Chakraborty[a],R.M. Chatterjee[a],S.K. Gupta[a],B. Hariharan[a],Y. Hayashi[b],P. Jagadeesan[a],A. Jain[a],H. Kojima[c],S. Kawakami[d],P.K. Mohanty[a],Y. Muraki[e],P.K. Nayak[a],T. Nonaka[f],A. Oshima[c],D. Pattanaik[a],S. Paul[a],M. Rameez[a],K. Ramesh[a],S. Rout[a],S. Sarkar[a],S. Shibata[c],M. Talwar[a],K. Tanaka[g],F. Varsi[a] – The GRAPES-3 Collaboration[†]

[a] *Tata Institute of Fundamental Research, Mumbai, India*
[b] *Osaka City University, Graduate School of Science, Japan*
[c] *Chubu University, College of Engineering, Japan*
[d] *Osaka City University, Graduate School of Science, Japan*
[e] *Nagoya University, Institute for Space-Earth Environmental Research, Japan*
[f] *University of Tokyo, Institute for Cosmic Ray Research, Japan*
[g] *Hiroshima City University, Graduate School of Information Sciences, Japan*

E-mail: mk.mohankarthik@gmail.com

The GRAPES-3 experiment, located at an altitude of 2200 metres in, Ooty, Tamil Nadu, India (11.4°N, 76.7°E, 2200 m a.s.l.), records extensive air showers in the TeV–PeV energy range using an array of 400 plastic scintillator detectors arranged in a hexagonal grid over an area of 25,000 m^2, along with a 560 m^2 muon detector made of proportional counters. The latter allows showers initiated by γ-rays to be distinguished from those originating in Cosmic Rays. In this work, we compare the performance of different classes of deep learning algorithms against standard cut-based selection techniques in isolating a sample of γ-ray initiated showers from data gathered between 2017 and 2022. We report on a search for steady emission from the Crab Nebula.

39th International Cosmic Ray Conference (ICRC2025)
15–24 July 2025
Geneva, Switzerland

ICRC 2025
The Astroparticle Physics Conference
Geneva July 15-24, 2025

[†]URL: https://www.tifr.res.in/grapes3/
[*]Speaker

PoS(ICRC2025)706

1. Introduction

The study of Very High Energy (VHE) gamma rays provides critical insights into the regions and mechanisms responsible for the acceleration of cosmic rays to extreme energies. Gamma rays travel in straight lines from their sources, making them excellent probes of astrophysical particle accelerators such as supernova remnants, pulsar wind nebulae, and active galactic nuclei. Their detection offers direct insight into environments where particles reach TeV–PeV energies.

The Crab Nebula, the remnant of a supernova explosion observed in 1054 A.D., is one of the most well-studied astrophysical sources across the electromagnetic spectrum. Powered by the central pulsar, the nebula emits non-thermal radiation via synchrotron and inverse Compton processes, extending from radio wavelengths up to PeV energies. Recently, the HAWC collaboration has reported the detection of gamma-ray emission from the Crab extending beyond 100 TeV [1], while LHAASO has reported similar detection upto PeV energies [2], confirming the Crab as a galactic PeVatron.

Due to its brightness, spectral stability, and well-understood emission profile, the Crab Nebula is widely used as a standard reference source for calibrating and validating gamma-ray observatories. This work presents the methodologies and results of utilizing Crab Nebula observations to assess and benchmark the sensitivity and performance of the **G**amma **R**ay **A**stronomy at **P**eV **E**nergie**S** Phase-**3** (GRAPES-3) experiment in the TeV energy range. Key components of the analysis include air shower reconstruction, data–simulation comparisons, gamma/hadron discrimination using Machine Learning (ML), and the application of statistical techniques to evaluate the significance of a point-like source.

2. The GRAPES-3 Experiment

The GRAPES-3 experiment, located at an altitude of 2200 metres in Ooty, Tamil Nadu, India (11.4°N, 76.7°E), is designed to study extensive air showers in the TeV–PeV energy range. It employs two primary detector systems: the GRAPES-3 Scintillator Detector array (G3SD) and the GRAPES-3 Muon Telescope (G3MT). The G3SD consists of 400 plastic scintillator detectors, each with an area of 1 m^2 and a thickness of 2–5 cm, arranged in a hexagonal grid with 8 m spacing between nearest neighbours, covering a total area of 25,000 m^2. The G3MT is composed of 16 modules, each containing four layers of proportional counters, with 58 counters per layer. Each proportional counter is 6 m long with a cross-sectional area of 10×10 cm^2. Consecutive layers are oriented orthogonally to enable muon tracking. A concrete absorber placed atop each module provides an energy threshold of $\sec(\theta)$ GeV for muons, where θ is the zenith angle, and is effective for incident angles up to 45°. This configuration allows the discrimination between air showers initiated by gamma rays and those produced by cosmic rays.

3. Data acquisition and pipeline

The G3SD subsystem generates the trigger for Extensive Air Shower (EAS) events by recording charge deposited and arrival times using charge-integrating qADCs and High Precision Time-to-Digital Converters (HPTDCs), respectively. A Level-0 trigger is issued based on a simple 3-line

coincidence window of 100ns, followed by a Level-1 trigger condition requiring at least 10 detectors to record a signal below -30mV within 1μs. These triggers initiate the recording of charge and timing information from all participating detectors. The charge is calibrated in the units of minimum ionizing particles (MIPs), and timing offsets are corrected relative to a reference detector. Further technical details are discussed in [3, 4].

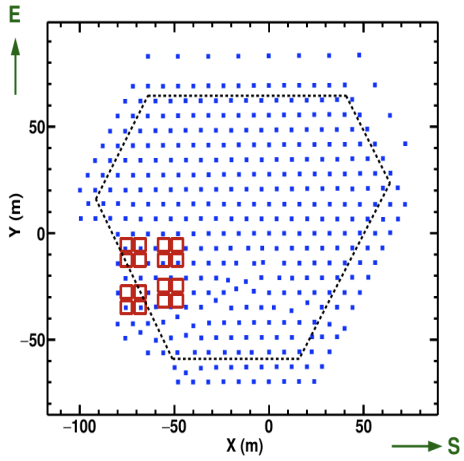

Figure 1: Schematic representation of the GRAPES-3 extensive air shower array. Scintillator detectors are represented by blue markers, while Muon Tracking modules are depicted as red squares. The dashed line indicates the fiducial area.

3.1 Reconstruction of Extensive Air Showers (EAS)

The primary properties reconstructed for each air shower include the direction, core position, shower size N_e, and shower age s. The shower direction is estimated by fitting a plane to the arrival times at various detectors using:

$$\chi^2 = \sum_{i=1}^{N} (lx_i + my_i + nz_i - c(t_i - t_0))^2 , \quad \text{with} \quad \sqrt{l^2 + m^2 + n^2} = 1 \tag{1}$$

The lateral distribution of particle densities is modeled using the NKG function [5]:

$$\rho(r_i) = C \left(\frac{r_i}{r_M}\right)^{s-2} \left(1 + \frac{r_i}{r_M}\right)^{s-4.5} \tag{2}$$

where r_i is the perpendicular distance from the i^{th} detector to the shower axis. The parameters C, N_e, s, and the core coordinates are obtained by maximising the likelihood of the observed detector signals. Further curvature corrections and iterative plane fitting are performed to refine the direction reconstruction, as discussed in [4].

3.2 Event Selection

The following quality cuts are applied prior to the classification of showers as gamma-ray or cosmic-ray events. First, only those showers that successfully converge when fitted with the Nishimura–Kamata–Greisen (NKG) function using the Minuit Migrad algorithm [6] are retained. Next, events with reconstructed shower cores located within the fiducial area, indicated by the

dashed boundary in Figure 1, are selected. In addition, only showers with reconstructed zenith angles $\theta < 45^\circ$ are considered. Further cuts are imposed on the shower size: only events with $N_e > 10^{3.5}$ and an age parameter in the range $0.2 < s < 1.8$ are included in the final dataset. The distance-from-muon-station cut is defined such that, for a given shower size as obtained from the NKG fit, only those events whose reconstructed cores lie within a specified distance from a muon station are retained. This criterion is applied exclusively in the distance-based analysis, with further details provided in Ref. [7].

4. Data-Simulation Comparisons & Gamma Ray / Cosmic Ray Classifier

The expected Background simulation rate is estimated using the H4a cosmic ray composition model. In this study, extensive air showers are simulated for five representative primary elements: proton (H), helium (He), nitrogen (N), aluminium (Al), and iron (Fe), representing the major mass groups in cosmic rays. For comparison, experimental data collected over 12 days spanning the 12 months of 2022 is used.

The input parameters to the ML Algorithms described in section 7 include the number of MIPS in a single detector and the number of tracks in a muon module. Comparisons between data and simulation for these parameters are shown in Figures 2, 3, and 4.

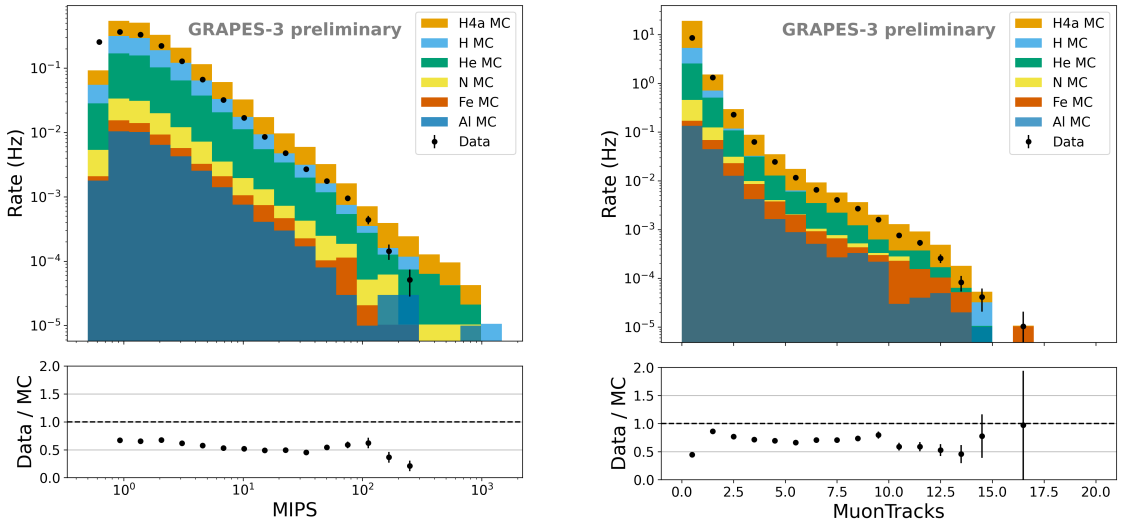

Figure 2: Distribution of MIPS count from plastic scintillator detector (left) and Distribution of Number of Muon Tracks in a single Muon Module. (right). This plot compares the distributions after the cuts mentioned in section 5 are applied.

The training datasets for the machine learning models are generated using CORSIKA [8] air-shower simulations (QGSJET-II.3 [9] for high-energy and FLUKA [10] for low-energy interactions), with the detector response modeled using GEANT4 [13]. Gamma-ray showers form the signal class, while proton, He, N, Al, and Fe primaries constitute the background. Events are simulated over 1, TeV–1, PeV and zenith angles up to 45°. The DNN takes 411 inputs: particle densities from 395 scintillators and muon counts from 16 modules. Its architecture has 4 hidden layers (128, 64, 32, 8

nodes) with batch normalization and dropout. ResNet-18 [14] is trained on $3 \times 224 \times 224$ images encoding particle densities, muon counts, and detector coordinates. Both models output a score in $[0, 1]$ representing the gamma-ray likelihood. When applied to real data (dominated by cosmic rays), score distributions are expected to follow background predictions from simulation. This is shown in Figure 3.

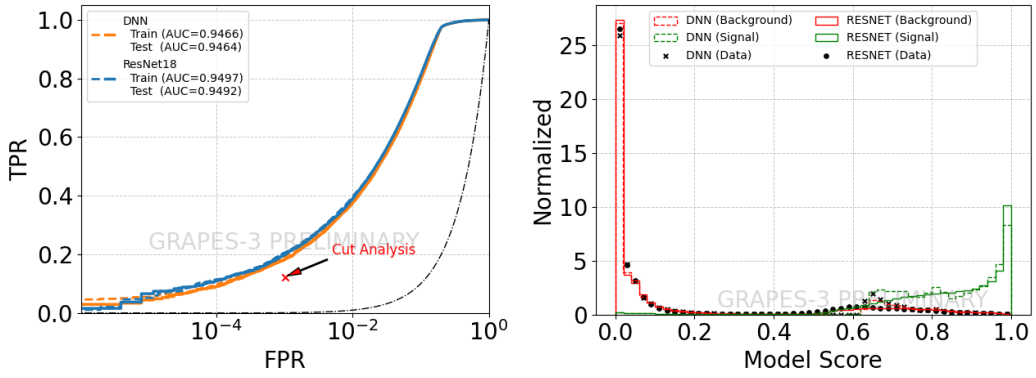

Figure 3: The Receiver Operating Characteristic (ROC) Curve on Train and Test simulation Set (left). The model score distribution for data and simulation (right). The Background simulation is weighted as per the H4a Model. The $\gamma-$ray signal simulation is also weighted to follow the same energy distribution as the background.

Table 1: Summary of event rates after applying Quality Cuts in Section 5 & Gamma/Hadron Cut

Cuts	**Simulation Diffuse Gamma Rate (Hz)**	**Simulation H4a Rate (Hz)**	**Data Rate (Hz)**
Trigger	8.11×10^{-4}	29.87	41.93
NKG Fit & $\theta_{rec} < 45°$	7.82×10^{-4}	27.06	37.83
Fiducial	6.17×10^{-4}	18.95	24.87
$0.2 <$ **Shower age** < 1.8	6.14×10^{-4}	18.66	24.27
Shower Size $> 10^{3.5}$	2.5×10^{-4}	10.60	10.29
Shower size dependent cut on distance from muon station (Only Cut Analysis)	2×10^{-5}	1.13	0.86
No. Muons = 0 (Only Cut Analysis)	2×10^{-5}	.011	.011
(DNN) Score > 0.977	2.29×10^{-5}	.0103	0.006
(RESNET - CNN) Score > 0.981	2.52×10^{-5}	.0103	-

In Table 1, we report the data and simulation event rates obtained after each successive quality cut. The performance of the ML models on both simulation and real data, following the gamma–hadron separation cut, is compared with that of the standard cut-based analysis. The background simulation rates are evaluated using the H4a composition differential flux model [15], while the diffuse gamma-ray simulation rates are estimated from the LHAASO measurement of the inner Galactic plane differential flux, $(1.00 \pm 0.04 \pm 0.09) \times 10^{-14} \left(\frac{E}{E_0}\right)^{-(2.99\pm0.04\pm0.07)}$, as reported in Ref. [16]. The first five rows summarise the event rates after the quality cuts, which are common

to both Cut-based and ML–based analyses. Cuts highlighted in red correspond to those applied exclusively in the cut-based analysis, while the orange and blue entries denote thresholds on the ML model scores, below which events are rejected. The threshold is chosen such that (False Positivity Rate) FPR of the models match the Cut-based Analysis.

5. Point Spread Function

The angular resolution of the primary particle direction in an air shower is evaluated by partitioning the triggered detectors into two independent subsets, based on odd and even numbering. Directional reconstruction, as outlined in Section 4, is then performed separately for each subset. The angular resolution is defined as half the angular separation between the two reconstructed directions. A precise determination of the angular resolution is crucial, as it characterizes the Point Spread Function (PSF), which is fundamental for the identification and localization of point-like gamma-ray sources.

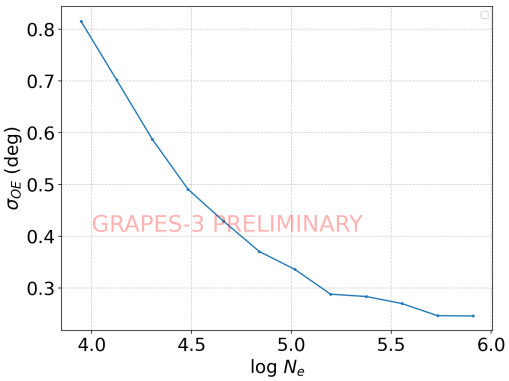

Figure 4: Angular resolution (68% containment radius) from Monte Carlo gamma-ray simulations as a function of shower size.

6. The unbinned Maximum Likelihood Ratio method

$$S_i = \frac{1}{2\pi\sigma_i^2} e^{-\frac{\psi^2(\delta_s,\alpha_s,\delta_i,\alpha_i)}{2*\sigma_i^2}} \quad (3)$$

$$B_i = \frac{1}{2\pi} P(\delta_i) \quad (4)$$

$$L = \Pi_i \frac{n}{N_{tot}} S_i + (1 - \frac{n}{N_{tot}}) B_i \quad (5)$$

$$H_0 : n = 0 \quad \text{vs.}$$
$$H_1 : n \neq 0 \quad (6)$$

$$T.S. = -2 \ln \frac{L(n=0)}{L(\hat{n})} \sim \chi_1^2 \quad (7)$$

(if H_0 true, Wilk's Theorem)

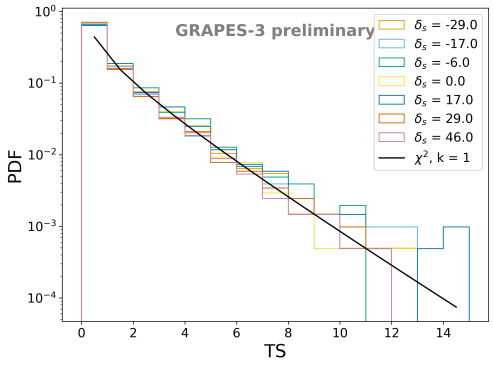

Figure 5: Test statistic distribution under the null hypothesis (H_0) as a function of source declination δ.

The likelihood method of Ref. [12] is adopted to assess the significance of candidate gamma-ray sources. In this framework, the signal is modeled as a two-dimensional Gaussian distribution centered on the source position, defined in terms of the angular separation $\psi(\delta_s, \alpha_s, \delta_i, \alpha_i)$ between the assumed source coordinates (α_s, δ_s) and the reconstructed event directions (α_i, δ_i). The width of the distribution is determined by the event-wise angular resolution σ_i, leading to the functional form 3. The background is taken to be uniform in right ascension, with a declination-dependent distribution $P(\delta_i)$ estimated from data. The likelihood is maximized with respect to n,

the number of signal events, and the test statistic (T.S.) is defined as the log-likelihood ratio between the background-only and signal-plus-background hypotheses. The null distribution (Figure 5) is obtained from pseudo-experiments generated by scrambling right ascension values while preserving detector effects. The resulting distribution is consistent with a χ^2 function with one degree of freedom, as shown in Figure 5, thereby validating the background model and enabling significance estimation.

7. Results

Gamma-like events from 2017–2022 were selected using a DNN score threshold of 0.98. A likelihood scan was carried out over a grid in right ascension (81.6°–85.6°) and declination (20°–24°) with a resolution of 0.05°. The resulting significance map (Fig. 6) exhibits a peak significance of 3.1σ at $83.48°, 22.21°$, at an offset of 0.24° from the Crab position reported by the H.E.S.S. collaboration. The significance was evaluated under the assumption that the null hypothesis follows a χ^2 distribution with one degree of freedom, as shown in Fig. 5. The observed offset, being within the angular resolution of GRAPES-3 (Fig. 4), may be attributed to a statistical fluctuation.

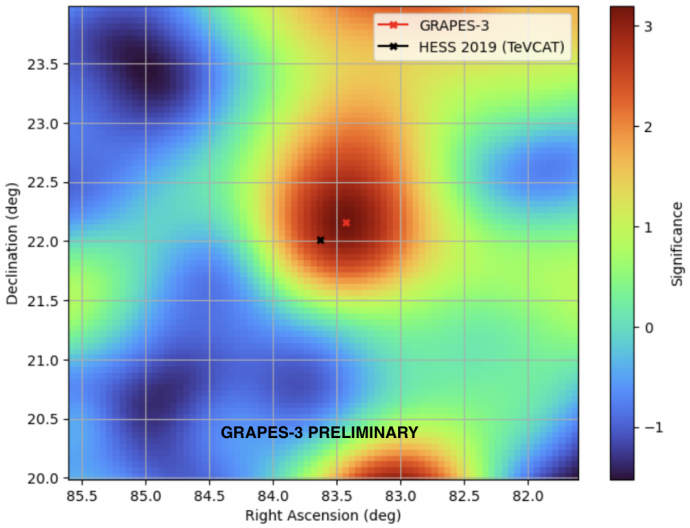

Figure 6: Significance map of the Crab Nebula region on a $4° \times 4°$ grid with 0.05° resolution

8. Conclusions

We have presented an update on efforts towards isolating a sample dominated by gamma-ray initiated showers using the combination of data acquired by both G3SD and G3MT. Studies are under way to further refine the machine learning models and analyses, while the final event selection is being further optimized. Estimating the spectrum of the Crab Nebula will provide a crucial calibration, establishing GRAPES-3 as a gamma-ray observatory.

Acknowledgment

I extend my sincere gratitude to the entire GRAPES-3 team for their unwavering efforts in maintaining the experiment and ensuring the integrity and quality of the data. This includes Dr. D. B. Arjunan, Mr. Manjunath, Mr. K. Ramesh, Mr. Himanshu, Mr. Rupesh, Mr. B. Rajesh, Mr. S. Murugapandian, Mr. R. Suresh Kumar, Mr. V. Santhosh Kumar, Mr. S. Kingston, Mr. S. Sheriff, Mrs. C. Shobana, Mr. Pandurangan, Mr. Vigneswaran, Mr. B. Vivek, Mr. Sreeganth, Mr. V. Jeyakumar, Mr. Arun, Mr. Dinesh, Mr. Vinoth, Mr. A. Charles, Mrs. B. Ganga, and Mrs. Rani. I acknowledge the use of the TIFR High Performance Computing (HPC) facility for the computational tasks involved in this work. We acknowledge the support of the Department of Atomic Energy, Government of India, under Project Identification No. RTI4002. Finally, I gratefully acknowledge the support of the Infosys–TIFR Leading Edge Travel Grant for funding to present this work at ICRC-2025.

References

[1] A. U. Abeysekara *et al.* (HAWC Collaboration),*Measurement of the Crab Nebula at the Highest Energies with HAWC*, Astrophysical Journal, Volume 881, 2019, Page 134, https://doi.org/10.3847/1538-4357/ab2f7d.

[2] Z. Cao *et al.* (LHAASO Collaboration), *Peta–electron volt gamma-ray emission from the Crab Nebula*, Science, Volume 373, Number 6553, 2021, Pages 425–430, https://doi.org/10.1126/science.abg5137.

[3] S. K. Gupta *et al.*, *The current status of the GRAPES-3 extensive air shower experiment*,Nuclear Physics B - Proceedings Supplements, Volume 196, 2009, Pages 153–158,https://doi.org/10.1016/j.nuclphysbps.2009.09.027.

[4] V. B. Jhansi *et al.*, *The angular resolution of GRAPES-3 EAS array after improved timing and shower front curvature correction based on age and size*, JCAP **07** (2020) 024, arXiv:1911.04715, doi:10.1088/1475-7516/2020/07/024.

[5] K. Kamata and J. Nishimura, *The Lateral and the Angular Structure Functions of Electron Showers*, Progress of Theoretical Physics Supplement, Volume 6, 1958, Pages 93–155, https://doi.org/10.1143/PTPS.6.93.

[6] F. James and M. Roos, *Minuit: A System for Function Minimization and Analysis of the Parameter Errors and Correlations*, Comput. Phys. Commun., Volume 10, 1975, Pages 343–367, https://doi.org/10.1016/0010-4655(75)90039-9.

[7] D. Pattanaik, *Study of multi TeV gamma ray sources with GRAPES 3 experiment*, Ph.D. thesis, Department of Physics, Utkal University, India (2024).

[8] D. Heck, J. Knapp, J. N. Capdevielle, G. Schatz, and T. Thouw, *CORSIKA: A Monte Carlo code to simulate extensive air showers*, Report FZKA-6019, Forschungszentrum Karlsruhe (1998).

[9] S. Ostapchenko, *QGSJET-II: Results for extensive air showers*, Nuclear Physics B - Proceedings Supplements **151**, 147–150 (2006), doi:10.1016/j.nuclphysbps.2005.07.027,arXiv:astro-ph/0412591.

[10] G. Battistoni, T. Boehlen, F. Cerutti, P. W. Chin, L. S. Esposito, A. Fassò, A. Ferrari, A. Lechner, A. Empl, A. Mairani, A. Mereghetti, P. Garcia Ortega, J. Ranft, S. Roesler, P. R. Sala, V. Vlachoudis, and G. Smirnov,*Overview of the FLUKA code*,Annals of Nuclear Energy **82**, 10–18 (2015),doi:10.1016/j.anucene.2014.11.007.

[11] D. Pattanaik *et al.* (GRAPES-3 Collaboration), *Validating the improved angular resolution of the GRAPES-3 air shower array by observing the Moon shadow in cosmic rays*,Phys. Rev. D **106**, 022009 (2022), doi:10.1103/PhysRevD.106.022009.

[12] J. Braun, J. Dumm, F. De Palma, C. Finley, A. Karle, and T. Montaruli, *Methods for point source analysis in high energy neutrino telescopes*, Astroparticle Physics, Volume 29, Issue 4, 2008, Pages 299–305, https://doi.org/10.1016/j.astropartphys.2008.02.007.

[13] F. Varsi *et al.*,*A GEANT4 based simulation framework for the large area muon telescope of the GRAPES-3 experiment*, Journal of Instrumentation, Volume 18, Number 03, 2023, Page P03046, https://doi.org/10.1088/1748-0221/18/03/P03046.

[14] K. He, X. Zhang, S. Ren, and J. Sun, *Deep Residual Learning for Image Recognition*, arXiv preprint arXiv:1512.03385, 2015.

[15] T. K. Gaisser, T. Stanev, and S. Tilav, *Cosmic Ray Energy Spectrum from Measurements of Air Showers*,arXiv:1303.3565 [astro-ph.HE] (2013). https://arxiv.org/abs/1303.3565.

[16] LHAASO Collaboration (Z. Cao *et al.*),*Measurement of Ultra-High-Energy Diffuse Gamma-Ray Emission of the Galactic Plane from 10 TeV to 1 PeV with LHAASO-KM2A*, Phys. Rev. Lett. **131**, 151001 (2023). https://doi.org/10.1103/PhysRevLett.131.151001.

[17] H.E.S.S. Collaboration, H. Abdalla *et al.*, *Resolving the Crab pulsar wind nebula at teraelectronvolt energies*, arXiv:1909.09494 [astro-ph.HE], 2019. https://arxiv.org/abs/1909.09494.